Proceedings of ASME Turbo Expo 2011
GT2011
June 6-10, 2011, Vancouver, British Columbia, Canada

GT2011-46283

EXPERIMENTAL AND NUMERICAL INVESTIGATION OF MISTUNED AERODYNAMIC INFLUENCE COEFFICIENTS IN AN OSCILLATING LPT CASCADE

Nenad Glodic
Royal Institute of Technology
Department of Energy Technology
S - 10044 Stockholm, Sweden

Damian Vogt
Royal Institute of Technology
Department of Energy Technology
S - 10044 Stockholm, Sweden

Torsten Fransson
Royal Institute of Technology
Department of Energy Technology
S - 10044 Stockholm, Sweden

ABSTRACT

The effect of aerodynamic mistuning on the aerodynamic damping in an oscillating Low-Pressure Turbine (LPT) cascade is investigated. The considered aerodynamic mistuning is caused by blade-to-blade stagger angle variations. The study is carried out experimentally and numerically by employing the influence coefficient method. On the experimental side a sector cascade is used where one of the blades is made oscillating in three orthogonal modes. The unsteady blade surface pressure is acquired on the oscillating blade and two neighbour blades and reduced to aeroelastic stability data. By gradually de-staggering the oscillating blade, aerodynamically mistuned influence coefficients are acquired. On the numerical side full-scale time-marching RANS CFD simulations are performed using nominal and de-staggered blades. The study shows that variations in blade-to-blade stagger angle affect the aerodynamic influence coefficients and as a consequence overall aeroelastic stability. Whereas discrepancies are found in the exact prediction of mistuned influence coefficients compared to measured, the overall magnitude and trends are well captured.

INTRODUCTION

Aerodynamic mistuning refers to aerodynamic non-uniformities due to geometric asymmetries in a blade cascade. Although no structural properties of blades are being changed, both steady and unsteady loads on blades are affected. The asymmetries might appear in engine manufacturing process, within frames of manufacturing tolerance or assembly inaccuracies, as well as in-service wear or even Foreign Object Damage (FOD).

The majority of previous investigations related to mistuning phenomena were concentrated on studying structural rather than aerodynamic mistuning. Kaza and Kielb [1]; Bendiksen [2]; Crawley and Hall [3], investigated how structural mistuning can be used for suppressing flutter in cascades. The results from a few, more recent, studies [4] where high fidelity models including both structural and aerodynamical coupling were used, indicate that impact of structural coupling on the stabilizing effects of structural mistuning is large. Thereby the beneficial effect of structural mistuning on flutter stability is inhibited by the addition of structural coupling effects. This behaviour is caused by the increased spread in tuned frequency due to structural coupling, making the system less sensitive to mistuning. A recent probabilistic flutter study of a mistuned bladed disk conducted by Kielb et al. [5], presented a method for identifying beneficial structural mistuning patterns.

An early study on effects of aerodynamic mistuning carried out by Hoyniak [6], showed that alternating blade spacing has stabilizing effects. Sladojevic et al. [7] investigated the influence of stagger angle variation on aerodynamic damping and frequency shift. Large alternating stagger angle variations (2.0deg) were found to have destabilizing effect. Kielb et al. [8] addressed the phenomenon of aerodynamic asymmetries on a probabilistic basis. By perturbing aerodynamic coupling coefficient between individual blades in the blade rows both intentional (i.e. symmetry groups) and random asymmetries could be studied. It has been found that random aerodynamic perturbation could have destabilizing effect while single blade and alternating perturbations tend to suppress flutter. Stüer et al. [9] showed that the impact of aerodynamic mistuning, in this case alternating chord length, for a structurally coupled system resulted in no net stability gain. Ekici et al. [10] investigated the effect of aerodynamic asymmetries caused by alternate blade-to-blade spacing and alternate staggering on the aeroelastic stability of a linear cascade. It was found that alternating spacing improved stability of the system while alternating staggering, on the other hand, was shown to have either stabilizing or destabilizing effect, depending on the direction of miss-staggering. Vogt et al. [11] studied the influence of aerodynamic asymmetries on mode shape sensitivity of an oscillating LPT cascade. The aerodynamic asymmetric perturbation was employed in generic manner, using a perturbation data acquired at negative incidence off-design operation of the setup. It was identified that mode regions that showed greater dependence from asymmetries were torsion-bending types of modes with torsion centre away from the blade pressure side.

The present study aims towards determining the level of change in aeroelastic properties of an oscillating LP turbine blade row upon change in blade stagger angle. For the first time ever, as far as the authors are aware, the perturbed aerodynamic influence coefficients are obtained directly employing both experimental testing and numerical simulations. On the experimental side, data is acquired in an oscillating LPT cascade facility where the stagger angle of the oscillating blade is being varied. A set of perturbed influence coefficients is extracted from the midspan unsteady pressure data for the blade oscillating in three orthogonal modes (two bending and one torsion mode). On the numerical side, a full-scale 3D time marching RANS CFD model is used. The model spans 7 blades whereof one is made oscillating. After the validation on test data the model is used to study the change in unsteady aerodynamics induced by blade destaggering. Furthermore it is concluded whether the numerical model is applicable to capture the effects of induced aerodynamic mistuning.

NOMENCLATURE

A	blade oscillation amplitude, per-degree basis for 3D consideration, per millimeter (bending) and per radian (torsion), respectively, for 2D consideration (stability parameter)
c	blade chord
c_p	static pressure coefficient $c_p = \dfrac{p - p_{s,ref}}{p_{0,ref} - p_{s,ref}}$
$c_{k,ae}$	stiffness matrix element
$c_{g,ae}$	damping matrix element
$\hat{c}_p$	normalized unsteady pressure coefficient (complex) $\hat{c}_p = \dfrac{\hat{p}}{A \cdot p_{dyn,ref}}$
df	infinitesimal force component
ds	infinitesimal arcwise surface component
$\vec{e}_\zeta$	direction vector torsion mode
$\hat{F}$	complex force vector
G	aerodynamic damping matrix
$\hat{\vec{h}}$	complex mode shape vector
h_i	oscillation amplitude
i	imaginary unit
k	reduced frequency
n, m	blade indices
$\vec{n}$	normal vector to surface element
N	number of blades
p	pressure
$\hat{p}$	unsteady pressure amplitude (complex)
$\vec{r}$	distance from center of torsion to force realization point
u	absolute outflow velocity
x, y, z	Cartesian coordinates
W_i	work per cycle

Greek symbols

λ	eigenvalue
σ	interblade phase angle
$\Delta\gamma$	de-stagger angle
ω	rotational frequency, rad/s
Ξ	stability parameter

Subscripts

ae	aerodynamic
dyn	dynamic
ic	influence coefficient
i	arbitrary mode
m	modal
ref	reference
twm	travelling wave mode

η	circumferential bending direction
ξ	axial bending direction
ζ	torsion direction

Abbreviations

IBPA	interblade phase angle
LPT	low pressure turbine
TWM	travelling wave mode
Im	imaginary part
Re	real part

THEORY

The present investigation is carried out in the influence coefficient domain where a single blade is oscillated while acquiring the unsteady blade surface pressure on the oscillating as well as the non-oscillating neighbour blades. The unsteady pressure response is of a complex nature indicating a phase shift between motion of the blade and aerodynamic response. In case of a tuned blade row and small oscillation amplitudes, the travelling wave mode response is obtained from linearly combining blade-specific influences as follows [11]

$$\hat{c}_{p,TWM}^{m,\sigma}(x,y,z) = \sum_{n=-\frac{N}{2}}^{n=+\frac{N}{2}} \hat{c}_{p,IC}^{n,m}(x,y,z) \cdot e^{-i\sigma n} \quad (1)$$

The travelling wave mode (TWM) contains contributions from all the blades and it assumes that all blades are oscillating in the same mode, at the same amplitude and frequency, but at a certain interblade phase angle σ. The right-hand side coefficients of the equation above are describing the influence coefficient domain while the left-hand side is describing the travelling wave mode domain. The described relation is only valid for the tuned blade row cases and small amplitudes.

The complex pressure coefficient yields from the unsteady pressure amplitude represented as a complex number and normalized by the reference dynamic head and the oscillation amplitude as follows

$$\hat{c}_p = \frac{\hat{p}}{A \cdot p_{dyn.ref}} \quad (2)$$

From the unsteady pressure coefficients the aerodynamic force coefficients are obtained by integration of infinitesimal local unsteady force components around the blade profile. Considering an orthogonal system of three modes the infinitesimal normalized force components per surface element ds are defined as

$$d\hat{f}_\xi = \hat{c}_p \cdot \vec{n}_\xi \cdot ds \quad (3)$$

$$d\hat{f}_\eta = \hat{c}_p \cdot \vec{n}_\eta \cdot ds \quad (4)$$

$$d\hat{m}_\zeta = (\vec{r} \times \hat{c}_p) \cdot \vec{e}_{\zeta_\perp} \cdot ds \quad (5)$$

The general force is given by integration

$$\hat{\vec{f}} = \oint d\hat{\vec{f}} \cdot ds \quad (6)$$

and aerodynamic force coefficient matrix can be defined as

$$\left[\hat{F}\right] = \begin{bmatrix} f_{\xi\xi} & f_{\xi\eta} & f_{\xi\zeta} \\ f_{\eta\xi} & f_{\eta\eta} & f_{\eta\zeta} \\ f_{\zeta\xi} & f_{\xi\eta} & f_{\zeta\zeta} \end{bmatrix} \quad (7)$$

In previous investigations ([13], [14]), it has been shown that the major influence in travelling wave mode response stems from the oscillating blade and its immediate neighbours (i, e, 0 and +-1). For blades with higher indices (+-2 and higher) the influence decays rapidly. While disregarding eventual acoustic resonances, this fact opens up for the possibility of using smaller models in influence coefficient domain (using sectors instead of spanning the entire circumference), which results in reduced computational time and simplifies the experimental setup. The minimum number of blades that must be included in the model needs to be decided carefully to ensure that the induced unsteadiness must damp out as the periodic boundaries are reached. The limited extent of the sector cascade employed in the present investigation was previously validated comparing to the travelling mode simulation results and was found to be sufficient for an accurate representation of the traveling wave mode response [16].

The harmonic motion of the oscillating blade is described by a complex mode shape vector $\hat{\vec{h}}$ with three orthogonal components $\{\hat{h}_\xi, \hat{h}_\eta, \hat{h}_\zeta\}$, describing axial bending, circumferential bending and torsion. The investigated orthogonal modes are shown in Figure 1.

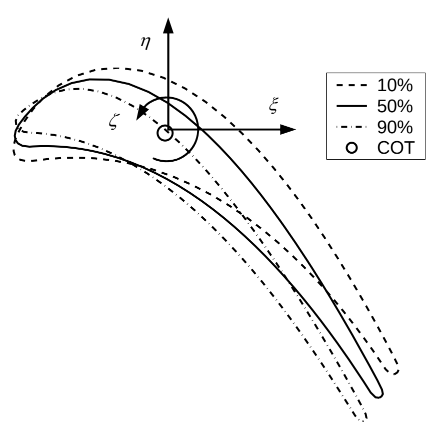

Figure 1. Basic orthogonal modes

Since the formulation given in Eq. 1 is only valid for a tuned setup, a model is needed that allows accounting for discrete changes in blade-to-blade aeroelastic properties. Herein a Reduced Order Model (ROM), in which the blades are reduced to single mass points, is used. The model is of cyclic character and has N degrees of freedom, where N corresponds to the number of blades. The aeroelastic equation of the system is given by

$$[M]\{\ddot{X}\}+[G]\{\dot{X}\}+[K]\{X\}=\{F_{ae}(t)\} \qquad (8)$$

where $[M]$ denotes the modal mass matrix, $[G]$ the modal damping matrix and $[K]$ the modal stiffness matrix. $\{X\}$ denotes the modal coordinate vector and $F_{ae}\{t\}$ is an aerodynamic excitation force vector. In the present work only aerodynamic damping forces are taken into account.

The aerodynamic damping forces are entirely motion dependent and are consequently moved to the left-hand side. After introducing a modal coordinate system

$$\{X(t)\}=[\varphi]\{\overline{Q}\}e^{i\omega\cdot t} \qquad (9)$$

and transformation into frequency domain the equation of motion is reformulated to an eigenvalue problem as follows

$$\left(-\varpi^2[M_m]+i\varpi[G_m-G_{ae}]+[K_m-K_{ae}]\right)\{\overline{Q}\}=0 \qquad (10)$$

where $[G_{ae}]$ denotes the aerodynamic damping matrix and $[K_{ae}]$ the aerodynamic stiffness matrix respectively. For a given mode the aerodynamic damping and stiffness matrices are populated by aerodynamic influence coefficients as follows

$$c_{k,ae_{n,m}}=\mathrm{Re}(f_{ic}^{n,m}),\ c_{g,ae_{n,m}}=\mathrm{Im}(f_{ic}^{n,m})\cdot\frac{1}{\omega} \qquad (11)$$

The aerodynamic matrices are of a diagonal character where the diagonal terms are the influence of the blades on themselves and the off-diagonal terms are containing influence of the neighbouring blades. The influence coefficient matrices in the present work are of tridiagonal type since only influences from blades -1, 0 and +1 are considered.

$$G_{ae}=\begin{bmatrix} c_{g,0,0}^{0} & c_{g,0,1}^{+1} & 0 & .. & c_{g,0,N-1}^{-1} \\ c_{g,1,0}^{-1} & c_{g,1,1}^{0} & c_{g,1,2}^{+1} & . & 0 \\ 0 & C_{g,2,1}^{-1} & C_{g,2,2}^{0} & . & 0 \\ . & . & . & . & . \\ 0 & 0 & 0 & . & c_{g,N-1,N-1}^{0} \end{bmatrix} \qquad (12)$$

Assuming a case where a single blade n is aerodynamically mistuned, it would imply that 3x3 of the coefficients in the aerodynamic matrix are affected i.e. matrix row containing blade *n*, but also the coefficients in rows $n-1$ and $n+1$ will be perturbed.

To describe aerodynamic damping of the system in accordance with previous work [14], an aerodynamic stability parameter Ξ [17] is used. The parameter presents the negative work per cycle normalized with the oscillation amplitude.

$$\Xi=\frac{-W_i}{\pi h_i}=-\mathrm{Im}(\hat{f}_i) \qquad (13)$$

Combining the eigenvalue solution given by

$$\lambda=-\frac{G}{2M}\pm i\cdot\sqrt{\frac{-G^2+4MK}{4M^2}} \qquad (14)$$

with the expression for the aerodynamic damping influence coefficient expressed in Eq.(11), a relation between the stability parameter and the eigenvalue solution is arrived as

$$\Xi=-\mathrm{Im}(\hat{f}_i)=2\cdot m\cdot\mathrm{Re}(\lambda)\cdot Abs(\lambda) \qquad (15)$$

DESCRIPTION OF THE TEST CASE

On the experimental side, an existing test facility at the Royal Institute of Technology in Stockholm was employed [15]. The test facility is shown in Figure 2. The facility contains an annular sector cascade of high subsonic LPT profiles. The test section comprises seven free-standing blades where one of the blades is made oscillating in three-dimensional orthogonal modes while the unsteady blade surface pressure is acquired on the oscillating blade itself (denoted as blade 0) and on the non-oscillating neighbour blades (blades ±1). Blade indices in the cascade are ascending in the direction of the suction side and descending in the direction of the pressure side respectively and range from -3 to +3. The blade profiles feature an aspect ratio of 1.94, a pitch-to-chord ratio of 0.68 and tip clearance of 1%. The cascade is here continuously operated at low subsonic velocity level (outlet Mach number of M_2=0.4.). During the tests the reduced frequency has been varied between k=0.1 and k=0.4. The stagger angle of the oscillating blade has been gradually varied within a range of -2.5 to +2.5deg. In practice the blade has been rotated by a certain de-stagger angle around the axis of the torsion mode.

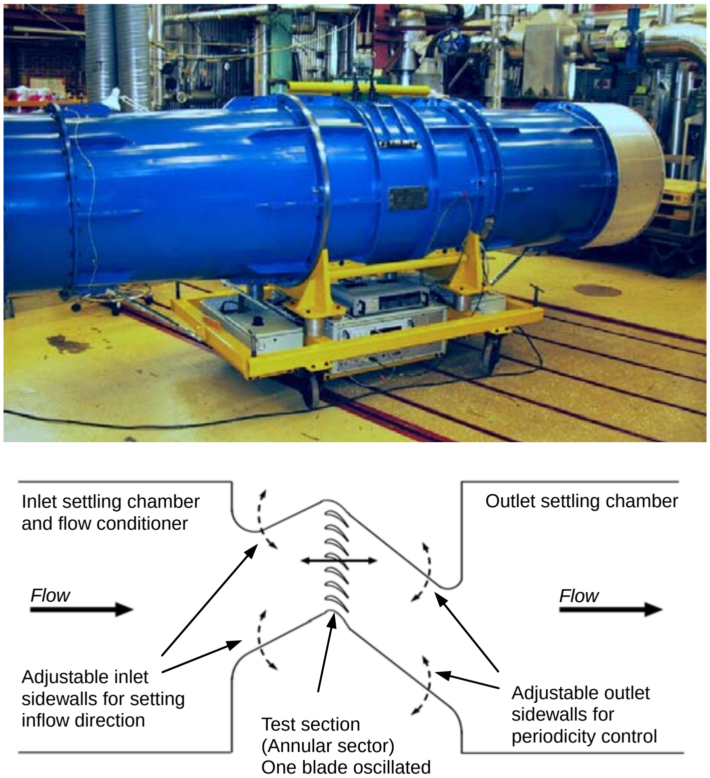

Figure 2. Test facility for aeroelastic investigation at KTH

Steady blade loading measurements have been performed employing multichannel PSI9116 pressure scanners with range of ± 105KPa at accuracy of ±52.5 Pa. Atmospheric pressure has been measured using SOLARTRON barometer with accuracy of ±11.5Pa. The unsteady blade surface pressure has been measured by means of fast-response pressure transducers that are mounted in a recessed manner. Taking into account accuracies of the sensor, resolution of the data acquisition system and transfer function accuracy, the total uncertainty for unsteady pressure measurements was determined to ±130 Pa [16], while uncertainty for unsteady pressure phase measurements was determined to ±20 degrees.

The oscillation of the blade in different mode shapes is achieved by employing a mechanical blade actuation mechanism. The mechanism contains two co-rotating circular eccentric cams, which induce a sinusoidal oscillatory movement of the blade. Change of stagger angle of the oscillating blade is achieved by turning the complete actuator clutched to the blade. The motion of the oscillating blade and pre-set stagger angle of the blade is thereby verified using point-wise laser vibration measurement system (OPTOCATOR). Accuracy of the oscillation amplitude measurements was determined to ±.05mm. The signal from the laser is acquired by means of a digital high-speed data acquisition system (Kayser Threde KT8000).

NUMERICAL METHOD

The cascade is modeled numerically by employing a commercial CFD code ANSYS CFX v.11 using a full-scale time-marching 3D viscous model. Previous investigations have shown potential of using the code for unsteady aerodynamics investigations [18]. The model extends over seven blades with periodic boundaries on the side walls. The simulations are conducted using a standard k-ε turbulence model with wall functions. In accordance with the experimental part the simulations are performed in the influence coefficient domain having only one blade oscillating. The motion of the oscillating blade is described by a set of equations and imposed as moving mesh boundary condition. De-staggering is applied in a similar manner: a set of equations is posed deforming the mesh on the target blade in each time step. The stagger angle is changed in the first time step of the simulation. Blade oscillation is thereafter introduced first after having the flow field around the de-staggered blade reaching a steady state. The blade is then oscillated for three oscillation periods. It has been found that the solution can be regarded as converged already after the second oscillation period (criterion used: < 0.5% phase-locked difference). The correctness of the imposed motion is confirmed by an analytical model. Data post-processing includes a reduction of time dependent data to complex unsteady pressures and calculation of aeroelastic stability data.

In order to obtain a required set of influence coefficients, in addition to the nominal case simulation, three more simulations per each investigated stagger angle have been performed: one simulation where destagger is applied on the oscillating blade and two additional simulations where each of the neighbouring blade was destaggered.

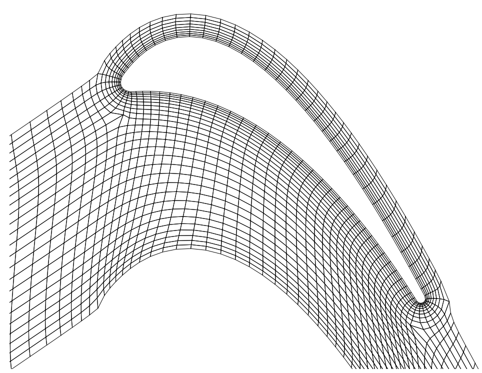

Figure 3. Mesh at midspan (one passage shown)

The 3D mesh employed in the simulations is generated using an in-house mesh generator and has previously been studied with respect to mesh sensitivity [19]. The grid is of multi-block type and contains both O- and H-blocks (Figure 3). The simulation domain consists of 507276 hexahedral volume elements with 540498 nodes. In order to optimize simulation effort, tip clearance has not been modelled. Results from previous investigations [18] have shown that models without tip clearance feature a more favourable convergence while the prediction accuracy at midspan is not affected considerably.

RESULTS

Steady blade loading

Steady blade loading data measured at the midspan of blades -1, 0 and +1 for various stagger angles of blade 0 is presented in Figure 5. The pressure coefficient is plotted against the normalized arcwise coordinate where the leading edge is located at the origin, with negative values spanning the suction side and positive values spanning the pressure side. Blade indices are included in the upper right corner of the respective graph.

A distinct suction peak is observed at arc=-0.11 followed by a slight deceleration towards aft suction side. On the pressure side the static pressure decreases monotonically from leading to trailing edge. The variation of the blade-to blade stagger angle leads to a change in passage throat. The affected passages are indicated in Figure 4. It is to be noted that a reduction in throat size leads to increased blockage and thereby increased pressure in the passage. On the other hand an increase in throat size leads to opening up the passage and consequently a decrease in pressure.

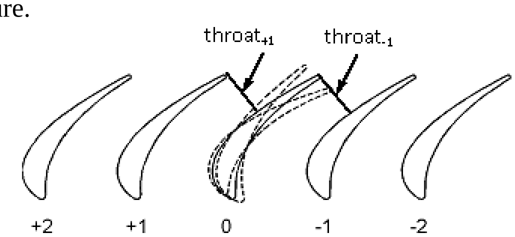

Figure 4. Impact of blade 0 de-staggering on passage throats

The observed suction peak is the most susceptible point when changing the blockage and the largest pressure change is observed at this location. The increased blockage in a passage weakens the pressure gradients around the peak and the peak becomes less pronounced, while for an increase in passage throat stronger gradients are present.

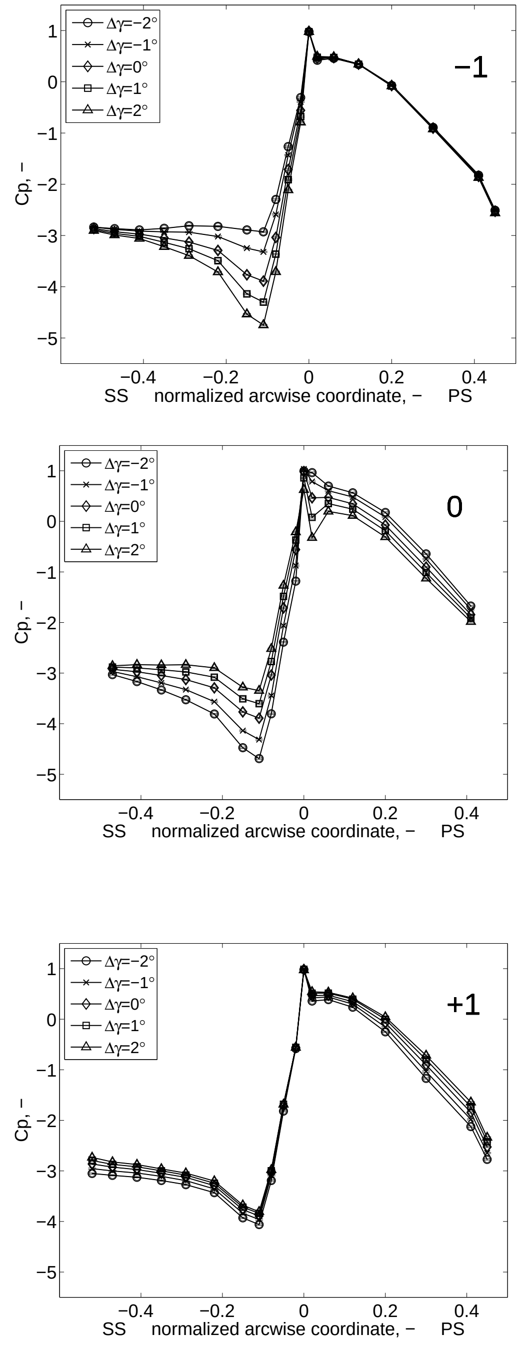

Figure 5. Steady blade loading data at midspan on blades -1, 0 and +1; M=0.4

Figure 6 depicts comparison of predicted and measured loadings at various destagger angles. It is observed that the predictions capture the changes in steady aerodynamics accurately. The agreement is equally good on the adjacent blades +1 and -1, which are not included here.

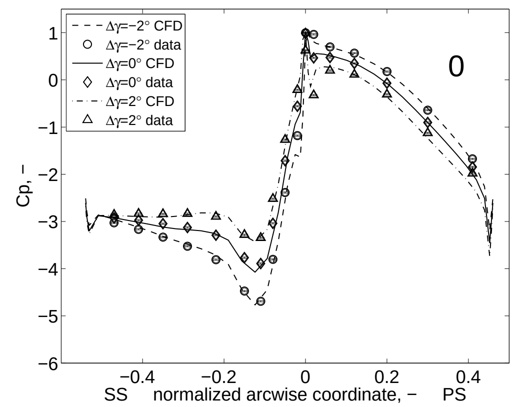

Figure 6. Steady blade loading at midspan on blade 0; test data vs. CFD; M_2=0.4

Unsteady response – nominal case

Unsteady response data is presented in the form of normalized unsteady pressure coefficients along the blade profile. The figures contain unsteady pressure amplitude plotted in the respective top window and the response phase in the bottom window. Unsteady blade loading test data and numerical results are contained in Figure 7 for blades -1 through +1 at axial bending mode. It is observed that on the suction side of blades 0 and -1 the response amplitude peaks around arc=-0.11, which was identified as the location of the suction peak in the steady blade loading. On blade +1 the major part of the response is observed on the pressure side facing the oscillating blade. The pressure phase suggests that the unsteady response primarily involves a flow passage and its respective surfaces. The unsteady pressure on the suction side of blade 0 and the pressure side of blade +1 is mainly in phase with the blade motion, while the pressure side on blade 0 and the suction side of blade -1 indicate opposite phase behaviour i.e. flow is 180deg out-of-phase. .

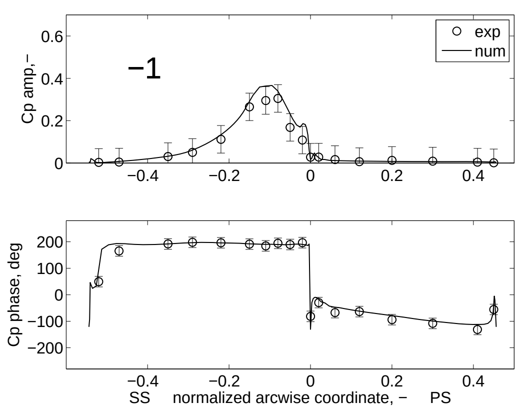

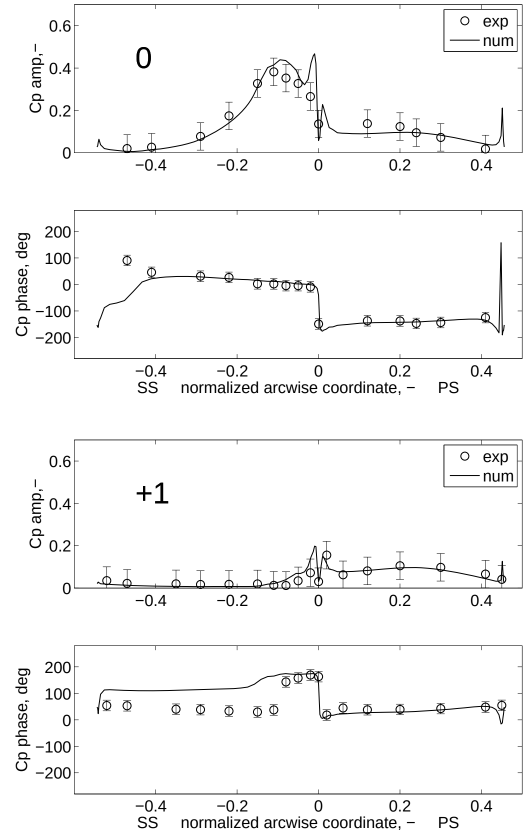

Figure 7. Unsteady blade surface pressure at midspan, axial bending, k=0.3 and M_2=0.4

Figure 7 indicates that both amplitude and phase of the response are well predicted by the numerical model. The response magnitude in the region of the suction peak on blades -1 and 0 is slightly over predicted by numerical model. Discrepancies in phase are observed on the aft suction side of blade 0 and aft suction side on blade +1; however the response amplitudes are very low in these regions. In general, the numerical model seems to capture the overall behaviour of the unsteady flow well.

Spatially resolved complex force coefficients are shown in Figure 8. The force component considered here is the unsteady force acting in the direction of the oscillation i.e. in this case the axial component. The imaginary and real parts of the force components are plotted against normalized arcwise coordinate. The numerical results generally correlate well to test data. Local differences are observed, especially in the imaginary force distribution on blade 0 and on the pressure side of blade +1. The real part of the force shows an overall good agreement between data and numerical results.

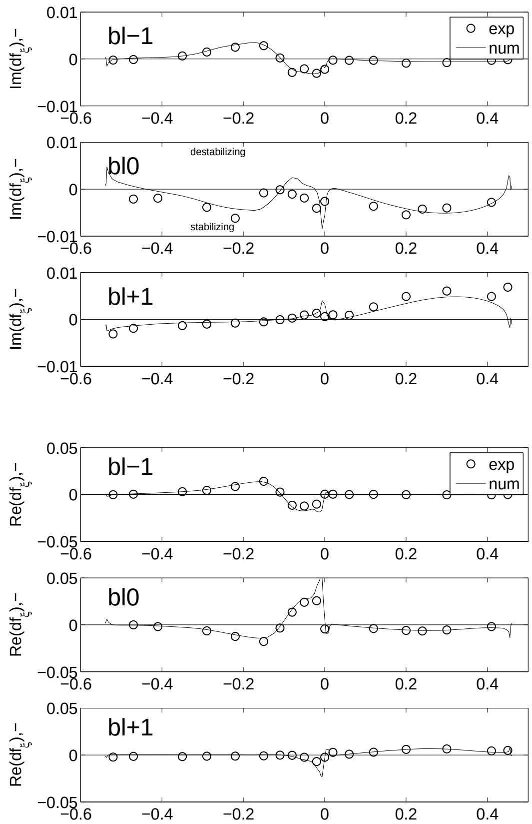

Figure 8. Resolved unsteady force component at midspan section on blades -1, 0 and +1 (imaginary and real)

The integrated aerodynamic force influence coefficients are presented in Figure 9. From an overall perspective there is a fair agreement between predicted and measured values. It is however apparent that relatively small differences in unsteady pressure magnitude and phase can translate into considerable differences in value of integrated force coefficients. The largest differences are observed for blade 0, where experimental data indicate a more stabilizing behaviour than predicted. A similar acceptable agreement between predicted and measured values was also observed for the two other investigated orthogonal modes (circumferential bending and torsion).

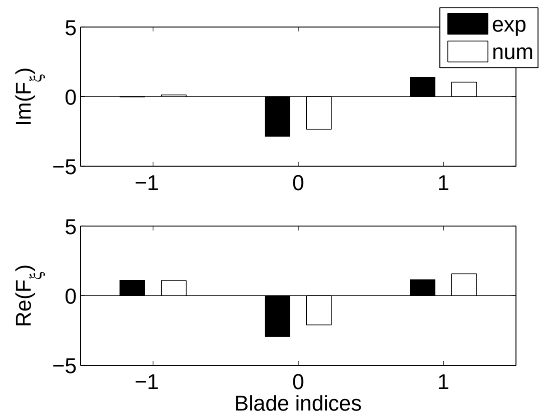

Figure 9. Nominal aerodynamic force influence coefficients for blades -1, 0 and +1; axial bending; k=0.3; M_2=0.4

Unsteady response- mistuned case

Figure 10 shows the unsteady pressure for the axial bending mode at reduced frequency of k=0.3 and outlet Mach number M_2=0.4. Two destaggered cases are shown, namely +2.5deg and -2.5deg. It is observed that the magnitude of the unsteady pressure coefficients changes moderately for the investigated de-stagger angles. Although distinct trends are measured, it is noticeable that these are in the order of magnitude of the measurement accuracy of the test setup. However, the observed trends are considered statistically significant since the measurements are performed with good repeatability. The effects of aerodynamic mistuning on aeroelastic properties are of less magnitude than the changes observed due to for example mode shape variations.

The largest change in magnitude is observed around the suction peak (around arc=-0.11) on the blades -1 and 0. The change in magnitude is consistent with the observed changes in blade loading i.e. increased blockage in passage +1 due to positive destaggering of blade 0 will results in lower response magnitude on the suction side of blade 0, since the velocity in the passage is lower and the gradients around the suction peak are weaker. Lower magnitude is also measured on the pressure side of blade +1. Opposite behaviour is noted for the negative destaggering. The phase of the response seems to be more affected by negative destaggering which is clearly seen on blade 0 where considerable phase deviation is present on the aft part on the suction side as well as a slight shift in phase on the pressure side. Similar phase deviation is also observed on the suction side on blade -1 and the pressure side on blade +1.

The phase variation on the suction side of blade +1 and the pressure side of blade -1 has a smaller significance since the response amplitude on these surfaces is very low.

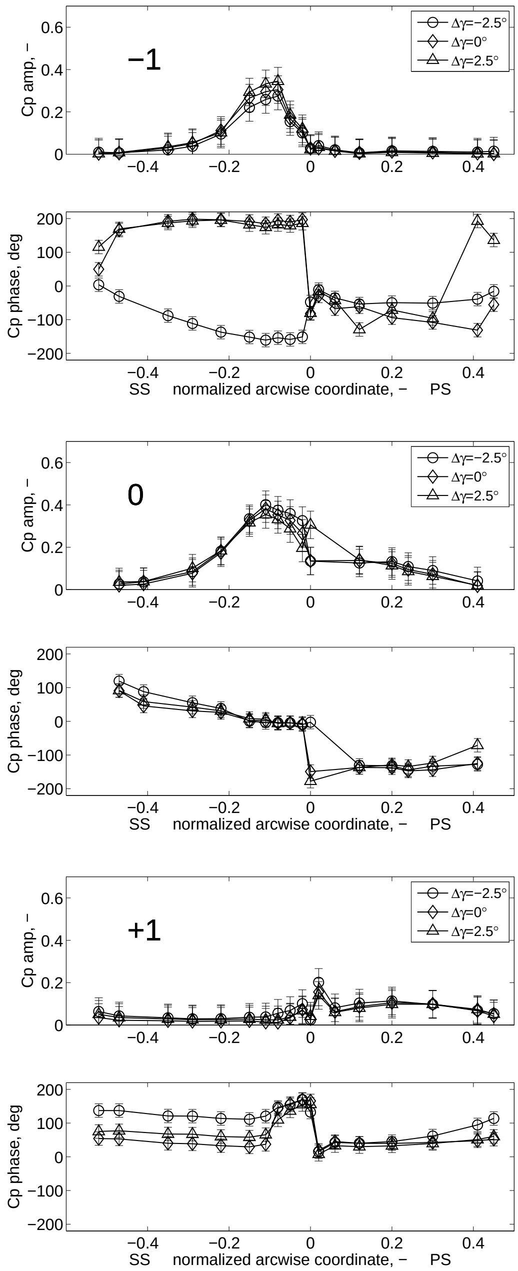

Figure 10. Unsteady pressure data at midspan on blades -1, 0 and +1; axial bending, k=0.3 and M_2=0.4;

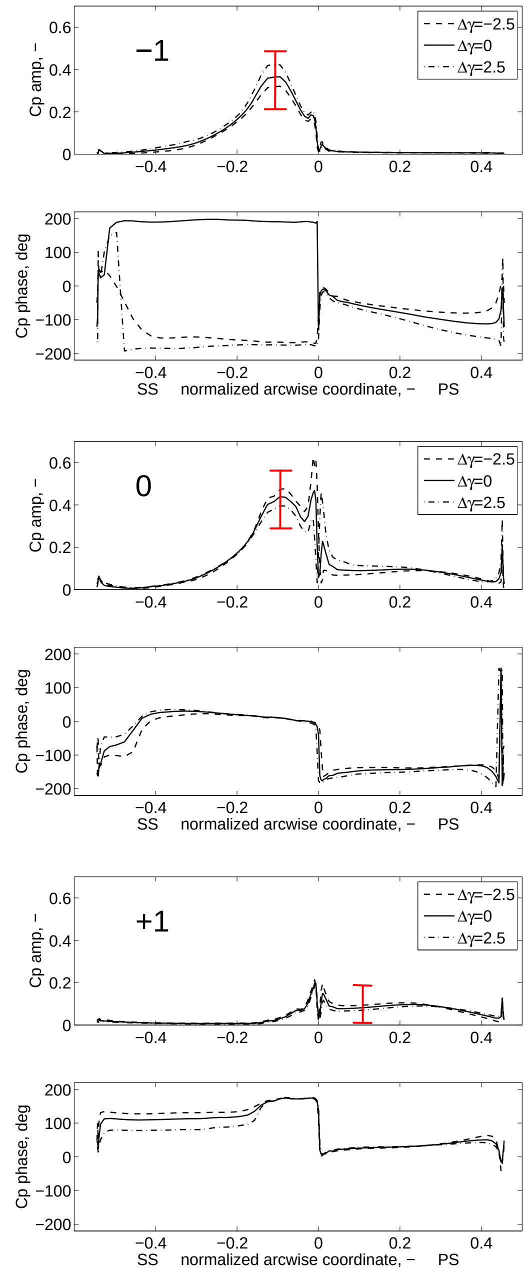

Figure 11. Numerical results for unsteady blade surface pressure distribution; axial bending, k=0.3 and M_2=0.4; red line indicates position of trend lines included below

In agreement with the experimental data, numerical results show that the most affected regions are located around the suction peak on the blade -1 and fore part of the blade 0. Figure 11 shows the unsteady response obtained from the numerical simulations. Predicted phase variations on blade 0 are not as pronounced as it was observed in the measured unsteady response data. It is observed that the change in response magnitude is well captured by the numerical model.

To be able to look more closely into the trends of response magnitude variation, Figure 12 depicts unsteady pressure magnitudes at the above marked locations that are most susceptible to changes. Same trends in magnitude variation can be observed in both numerical results and test data.

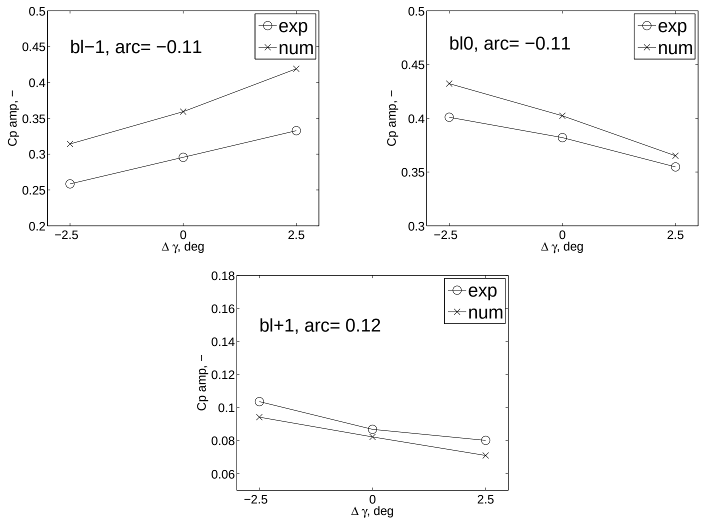

Figure 12. Cp amplitudes at specific locations on blades -1, 0 and +1; axial bending, k=0.3 and M_2=0.4

Mistuned aerodynamic influence coefficients

In order to analyse the impact of the blade 0 stagger angle variation on the influence coefficients, the complex force coefficients are plotted in the complex plane as included in Figure 13. The influence coefficients determined for the different stagger angles and blades are marked with markers and enclosed within rectangles highlighting the region of the coefficient variability. It is observed that the influence coefficient obtained from data measured on blade 0 is considerably affected by the change of the stagger angle. Negative de-staggering seems to have the strongest impact, moving the influence coefficient to more negative values i.e. blade 0 tends to have a more stabilizing effect when negative de-stagger angles are applied.

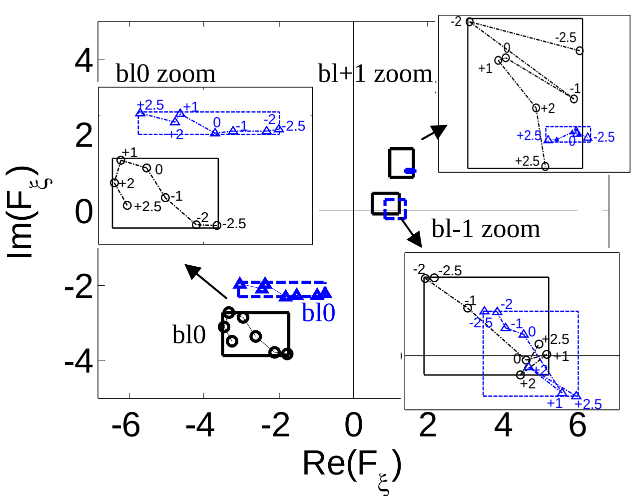

Figure 13. Mistuned influence coefficients for blades -1, 0 and +1; experimental data (black coloured) and numerical results (blue coloured); axial bending; k=0.3

The influence coefficients on the neighbouring blades seem to be less affected by the change of stagger angle variation. The spread of the numerically predicted coefficients, enclosed by blue dashed line rectangles, is generally less pronounced. The predicted influence variation for blade +1 is considerably smaller than the one measured. It is also noted that no clear trend in variation of the coefficients due to stagger angle change is apparent.

At this stage, a note shall be made on the prediction and measurement accuracy of complex force influence coefficients. Despite the fact that most of the complex pressure data points lie within the measurement accuracy, noticeable differences are apparent in the complex force influence coefficients. The reason for this behaviour is to be found in the integration of complex blade surface pressure with respect to a specific orthogonal mode. Thereby, three ingredients play a role: i) the local unsteady pressure magnitude, ii) its phase and iii) the local blade shape. Hence, seemingly small and local deviations in i) and/or ii) might have a major impact on the integrated values depending on their location. This observation applies to both experiments and predictions. As the effects are of systematic nature, the findings of the present study in terms of variability of force influence coefficients are however not affected by this observation.

The impact of the reduced frequency is addressed in Figure 14. The same range of de-stagger angles (within ±2.5deg) was tested at each reduced frequency. The perturbation of the blade 0 influence coefficient seems to grow with increased frequency and at the same time the coefficients move to more negative values meaning that blade 0 obtains more stabilizing character. Values and size of the rectangles for blade -1 does not change significantly with reduced frequency and influence coefficients remain small. The variability region for blade +1 moves to more positive values with an increase in reduced frequency.

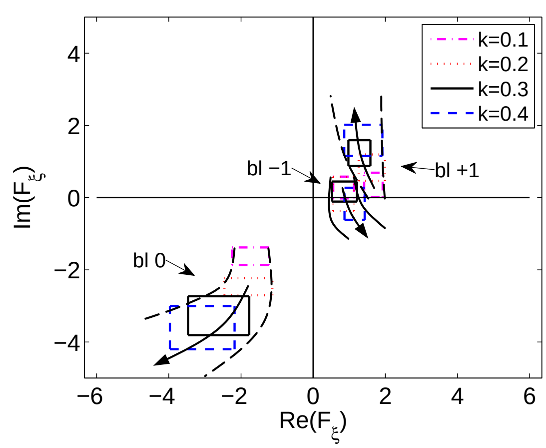

Figure 14. Mistuned influence coefficients vs. reduced frequency; axial bending; M_2=0.4; experimental data

Similar behaviour can be observed for the circumferential bending and the torsional mode that are depicted in Figure 15 and Figure 16 respectively. Deviations of the influence coefficients on neighbouring blades for the torsional mode seem to be much less affected than what is observed for the bending modes. The variability of blade 0 shows a growing trend with increase in reduced frequency.

A comprehensive study of mistuned influence coefficients at different reduced frequencies, mode shapes and velocity levels led to the conclusion that no clear general trend in change of influence coefficients with stagger variation could be identified. Therefore enclosed deviation regions shown here should be taken rather as a perturbation basis for a probabilistic treatment of mistuned assemblies under assumption that if an applied stagger variation is within boundaries of the here investigated angles, influence coefficients will change inside the marked regions. This opens up for the probabilistic analysis of the flutter stability.

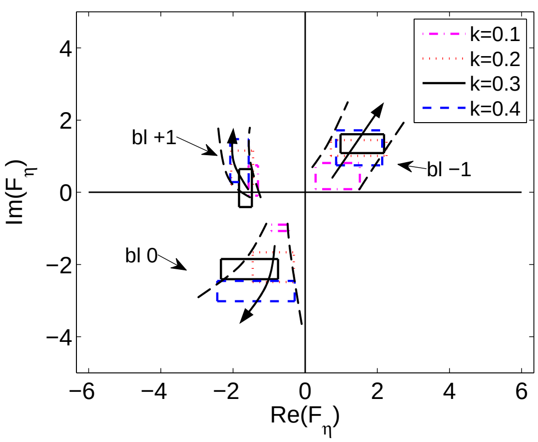

Figure 15. Mistuned influence coefficients vs. reduced frequency; circumferential bending; M_2=0.4; experimental data

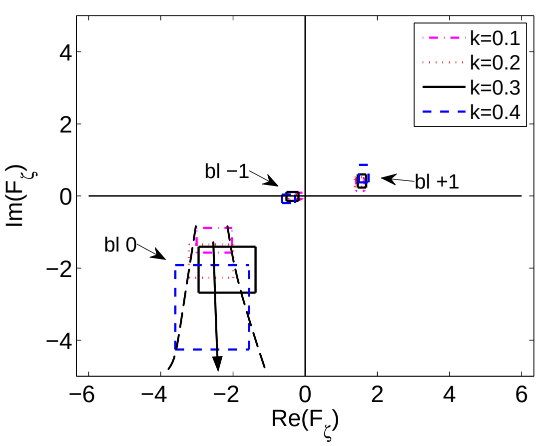

Figure 16. Mistuned influence coefficients vs. reduced frequency; torsion; M_2=0.4; experimental data

<u>Mistuned aeroelastic model</u>

On the background of experimental data a numerical model for assessing the aeroelastic stability of aerodynamically mistuned blade rows is composed. It has been shown above that the numerical model used is capable of predicting the trends and to a large degree also the levels of aerodynamic mistuning based on blade 0 destagger data. From this it is concluded that the numerical model is equally applicable for correctly predicting the changes in aeroelastic properties due to blades +1 and -1 respectively being destaggered.

In order to assess the overall aeroelastic stability of a randomly mistuned blade row, the aforementioned ROM model is built on a probabilistic basis. A fleet of 1000 blade rows is regarded in which every 5th blade (i.e. 20% of all blades) is destagger at a random angle between -2.5deg and +2.5deg. In this way spacing between the de-staggered blades is sufficient to assume that the influence of two de-staggered blades is not affecting each other. The result included here focuses on the axial mode and reduced frequency k=0.3 and is shown in terms of S-curve as well as cumulative probability.

Fig 17 shows the S-curve of the nominal (i.e. tuned) setup based on linear superposition as well as the discrete ROM model introduced above. The two curves are in line showing the validity of the ROM model. In addition the stability of the mistuned blade rows is included as a point cloud. It is apparent that the effects on stability are not very drastic amounting to about 15% of the S-curve peak-to-peak amplitude. With respect to the least stable mode it is observed that changes are very small and do not represent a significant danger for having the setup destabilized.

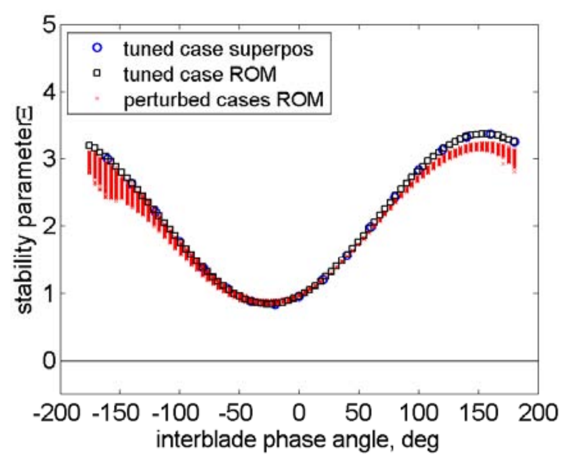

Figure 17. Effect of random mistuning on flutter stability; 20% of blades de-staggered; numerical results

The cumulative probability of the least stable mode is included in Fig 18. It is apparent that the majority of the mistuned setups feature higher aeroelastic stability than tuned. 14% of the regarded fleet however features a minimum stability that is lower than tuned. With respect to the peak-to-peak amplitude of the tuned setup the variability in the least stable mode is less than 3%.

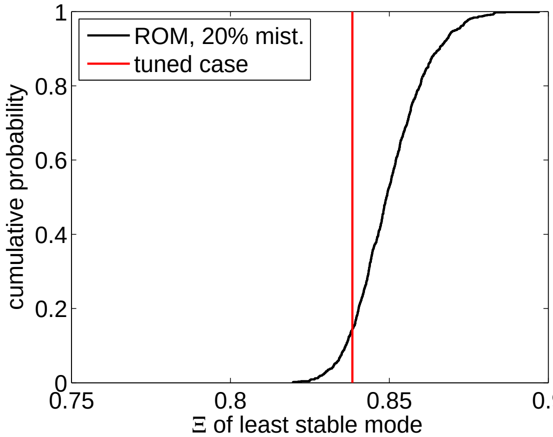

Figure 18. Cumulative probability of least stable mode

CONCLUSIONS

The effect of aerodynamic mistuning on the aeroelastic stability of an oscillating LPT cascade has been investigated experimentally and numerically. Aerodynamic mistuning has thereby been introduced as blade-to-blade stagger angle variation. The study has been performed using the influence coefficient method in which the influence coefficients directly have been measured and predicted respectively and reassembled such as to yield travelling wave mode results. A set of three orthogonal modes has been investigated (two bending and one torsion mode).

The effect of destaggering a single blade on steady aerodynamics has been explained from test data. The observed effects seem to be predominantly an effect of the change in passage throat. The changes in steady aerodynamics are observed on the unsteady aerodynamics where distinctive effects on flow velocity lead to changes in local unsteady pressure coefficients.

Correlation of numerical results to test data with having one blade destaggered leads to the following conclusions:

- The numerical model used is capable of accurately capturing the differences in steady aerodynamics induced by the destaggering
- The trends in change of unsteady pressure response during blade oscillation due to destaggering are generally well captured. Moderate differences are observed in the absolute values of response amplitude and phase however
- There is no clear trend in complex integrated force influence coefficients, neither in test data nor in numerical results
- The numerical model tends to predict a moderately smaller variability of influence coefficients with destagger than measured
- Trends with reduced frequency show that the variability due to destagger increases for all modes. Blade 0 shows an increasingly stabilizing behaviour with increase in reduced frequency, which confirms the finding from previous studies ([13], [14], [20]).

After having validated the numerical model, a ROM model has been built to address the aeroelastic stability of randomly mistuned blade rows. The ROM model takes into account mistuned aerodynamic stiffness and damping coefficients. For the present study, the influence coefficients of blades -1, 0 and +1 only have been regarded. These coefficients have been acquired from three individual simulations with having blade -1, 0 and +1 respectively destaggered. The ROM model has been used to perform a probabilistic analysis of the effect of aerodynamically mistuned influence coefficients involving a fleet of 1000 blade rows leading to the following conclusions:

- The effect of the present type of aerodynamic mistuning is of moderate nature and amounts to an average of about 15% of the stability curve (peak-to-peak) amplitude
- The majority of the randomly mistuned blade rows feature higher minimum aeroelastic stability than nominal. 14% feature a lower stability
- The overall variations in minimum stability amount to 3% of the stability curve (peak-to-peak) amplitude
- The effects of aerodynamic mistuning on the interblade phase angle at minimum stability can be neglected

Based on the above conclusions, it is stated that the investigated type of mistuning can lead to a measurable even though only moderate change in aeroelastic stability. In the light of industrial practices this means the following:

- As long as the geometrical blade-to-blade variations in stagger angle are within a range of +-2.5deg the negative effects of aerodynamic mistuning on aeroelastic stability can be taken care of by applying a certain safety margin. For the present type of turbomachine cascade, this safety margin is given as 5% peak-to-peak amplitude of the stability curve
- Most probably structural mistuning would outbalance any destabilizing effect due to aerodynamic mistuning

ACKNOWLEDGMENTS

The present study has been funded by the Swedish Energy Agency, Siemens Industrial Turbomachinery AB, Volvo Aero Corporation, and the Royal Institute of Technology through the Swedish research program TURBOPOWER, the support of which is gratefully acknowledged.

REFERENCES

[1] Kaza, K.; Kielb, R. E.; 1983, "Aeroelastic Characteristics of a Cascade of Mistuned Blades in Subsonic and Supersonic Flows", Journal of Vibration, Acoustics, Stress and Reliability in Design, Vol.105, October 1983

[2] Bendiksen, O., 1984, "Flutter of Mistuned Turbomachinery Rotors", ASME Paper No 83-GT-153

[3] Crawley, E. F.; Hall, K. C., 1985, "Optimization and Mechanism of Mistuning in Cascades", Journal of Engineering for Gas Turbines and Power, 108

[4] Kielb, R. E.; Feiner, D. M.; Griffin, J. H.,; Miyakozawa, T.; 2004, "Flutter of Mistuned Bladed Disks and Blisks with Aerodynamic and FMM Structural Coupling", ASME GT-2004-54315, Vienna, Austria, June 2004

[5] Kielb, R. E., Hall, K. C., 2006, "Probabilistic Flutter analysis of Mistuned Bladed Disk", ASME Paper GT2006-90847

[6] Hoyniak, D., 1986, "The effect of circumferential aerodynamic detuning on coupled bending-torsion unstalled supersonic flutter", Journal of turbomachinery, Nr.2, Vol.108

[7] Sladojevic, I., Sayma A. I., Imregun M., 2007, "Influence of Stagger Angle Variation on Aerodynamic Damping and Frequency Shifts", ASME paper GT2007-28166

[8] Kielb, R. E., Hall, K. C., Miyakozawa, T., 2007, "The effect of Unsteady Aerodynamic Asymmetric Perturbations on Flutter", ASME Paper GT2007-27503

[9] Stüer, H., Schmitt, S., Ashcroft, G., 2008,],["Aerodynamic Mistuning of Structurally Coupled Blades", A]SME Paper GT2008-50204

[10] Ekici, K; Kielb, R., E.; Hall, K. C.; 2008, "Aerodynamic Asymmetry Analysis of Unsteady Flows in Turbomachinery", ASME Paper GT2008-51176

[11] Crawley, E.F., 1988, "Aeroelastic Formulation for Tuned and Mistuned Rotors", AGARD Manual on Aeroelasticity in Axial-Flow Turbomachines, Vol . 2, Structural Dynamics and Aeroelasticity, Chapter 19, AGARD-AG-298

[12] Vogt, D.M., Glodic, N., Fransson T. H., 2009, "The Effect of Unsteady Aerodynamic Asymmetric Perturbations on the Mode Shape Sensitivity of an oscillating LPT Cascade", ISUAAAT 12 paper

[13] Panovsky, J. and Kielb, R., 2000, "A Design Method to Prevent Low Pressure Turbine Blade Flutter", Journal of Engineering for Gas Turbines and Power, Vol.122, January 2000

[14] Vogt, D.M., Fransson, T. H., 2007, "Experimental Investigation of Mode Shape Sensitivity of an Oscillating LPT Cascade at Design and Off-Design Conditions", ASME J. of Engineering for Gas Turbines and Power, 129, 2007, pp.530-541

[15] Vogt, D.M., Fransson, T. H., 2002, "A New Turbine Cascade for Aeromechanical Testing", Paper presented at the 16th Symposium on Measuring Techniques in Transonic and Supersonic Flows in Cascades and Turbomachines, Cambridge, UK

[16] Vogt, D. M., 2005," Experimental Investigations of Three-Dimensional Mechanisms in Low-Pressure Turbine Flutter", Doctoral Thesis, Royal Institute of Technology, Department of Energy Technology, Stockholm, 2005

[17] Verdon, J.M., 1987, "Linearized Unsteady Aerodynamic Theory", AGARD Manual on Aeroelasticity in Axial-Flow Turbomachines, Vol. 1, Unsteady Turbomachinery Aerodynamics, Chapter 2, AGARD-AG-298

[18] Vogt, D. M., Mårtensson, H.E., Fransson, T.H., 2007, "Direct Calculation of Aerodynamic Influence Coefficients Using a Commercial CFD Solver", Paper presented at the 18th ISABE Conference in Beijing, September 2-7, 2007

[19] Mårtensson, H, Vogt, D. M., Fransson, T. H., 2005, "Assessment of a 3D Linear Euler Flutter Prediction Tool Using Sector Cascade Test Data", Proceedings of ASME Turbo Expo 2005, GT2005-68453

[20] Nowinski, M. and Panovsky, J., 2000, "Flutter Mechanism in Low Pressure Turbine Blades", Journal of Engineering for Gas Turbines and Power, Vol.122, January 2000

